BBA Advances 4 (2023) 100110

Contents lists available at ScienceDirect

BBA Advances

journal homepage: www.sciencedirect.com/journal/bba-advances

Fibril core regions in engineered α-synuclein dimer are crucial for blocking of fibril elongation

Celina M. Schulz [a,1], Anne Pfitzer [a,1], Wolfgang Hoyer [a,b,*]

[a] Institut für Physikalische Biologie, Heinrich Heine University Düsseldorf, Düsseldorf, Germany
[b] Institute of Biological Information Processing (IBI-7: Structural Biochemistry) and JuStruct: Jülich Center for Structural Biology, Forschungszentrum Jülich, Jülich, Germany

ARTICLE INFO

Keywords:
α-Synuclein
Elongation
Fibrillation
Fibril polymorphs
Mechanism of inhibition
Amyloids

ABSTRACT

Synucleinopathies like Parkinson's disease are neurodegenerative diseases which are associated with the deposition of fibrillar aggregates of the endogenous protein α-synuclein (α-syn). The inhibition of the elongation of α-syn fibrils is of great scientific interest and an option in the design of therapeutic strategies. Previously, we developed a disulfide-containing mutant of α-syn, called CC48, which inhibits fibril elongation by blocking of fibril ends. Surprisingly, wildtype (WT) α-syn molecules supported the blocked state, and a fusion of CC48 with WT α-syn, denoted WT-CC48, exhibited increased inhibitory potential. Here, we studied which regions of WT-CC48 are responsible for the strong inhibitory effect. To this end, we investigated a set of truncated versions of WT-CC48 by kinetic elongation assays, density gradient centrifugation, and atomic force microscopy. We show that in both the WT and the CC48 part of the fusion construct the hairpin region (residue 32–60) and NAC region (61–95), but not N- and C-terminal regions, are required for strong inhibition of fibril elongation. The required regions correspond to the segments forming the β-sheet core of α-syn fibrils. As α-syn fibrils typically consist of two protofilaments, the dimeric construct WT-CC48 provides the critical regions sufficient to cover the full β-sheetcore interface exposed at the fibril end, which can explain its high inhibitory efficiency. We suggest a mechanistic model of CC48-mediated inhibition of fibril elongation in which CC48 and WT α-syn cooperatively form an oligomer-like cap at the amyloid fibril end.

Introduction

A large number of proteins and peptides have been shown to undergo aggregation processes resulting in the loss of function and the build-up of toxic debris [1–4]. The aggregates often consist of fibrils with a highly ordered β-sheet core, the so-called cross-β amyloid structure [5,6]. Amyloid fibril formation is associated with many diseases, including Alzheimer's disease and Parkinson's disease (PD) [7–9]. Synucleinopathies, like PD, are believed to be triggered by amyloid fibril formation of the 140 amino acid long presynaptic protein α-syn. In PD patients, it is found in Lewy bodies as insoluble inclusions [10,11].

α-syn can assemble into several distinct fibril structures, referred to as polymorphs, which were termed, e.g., ribbons, rod, and twister [12–15]. Almost all α-syn fibril polymorphs resolved structurally up to this day consist of two protofilaments. In all polymorphs, the central region of α-syn comprising amino acids 30–100 contributes the largest part of the cross-β fibril core. The precise fold of the α-syn units within the fibril core, however, can be quite variable among polymorphs, including diverse protofilament interfaces.

Amyloid formation can be described as a mechanism of nucleated polymerization and is a multistep process, comprising primary nucleation, secondary nucleation and elongation [16–18]. In the process of primary nucleation, monomers undergo a structural transformation to form growth-competent nuclei [19]. In secondary nucleation, oligomer formation and conversion to a fibril seed is catalyzed on the surface of a pre-existing fibril [18,20]. Elongation describes the binding of a monomer to a fibril end and the structural conversion of the newly attached molecule into the cross-β amyloid structure [20,21]. As elongation is a fundamental reaction step of fibril growth, fibril mass cannot be generated under conditions that prohibit elongation. Therefore, the fibril end is an interesting target site to achieve inhibition of elongation and fibril formation in general. Moreover, the number of fibril ends is

* Corresponding author at: Institut für Physikalische Biologie, Heinrich Heine University Düsseldorf, Düsseldorf, 40204 Düsseldorf, Germany.
E-mail address: wolfgang.hoyer@hhu.de (W. Hoyer).
[1] These authors contributed equally: Celina M. Schulz, Anne Pfitzer

https://doi.org/10.1016/j.bbadva.2023.100110
Received 31 August 2023; Received in revised form 20 October 2023; Accepted 9 November 2023
Available online 10 November 2023

low compared to that of aggregated protein units, which may support inhibitory activities at low inhibitor concentrations [22]. Different types of molecules have thus been designed and/or selected to occupy the fibril ends and block elongation, such as antibodies [23], peptides [24], or protein constructs [25–27].

Previously, our group introduced an α-syn double cysteine insertion mutant which specifically inhibits the elongation of wildtype (WT) α-syn fibrils [28,29]. The mutant, here called CC48, comprises the mutations of G41C and V48C allowing the formation of an intramolecular disulfide bond. The position of the disulfide bond was chosen to promote formation of a hairpin in the region comprising α-syn residues 32 to 60 (labeled here HP region, Fig. 1) that was observed upon binding to the engineered protein AS69. Several studies showed that this region is of critical importance for α-syn aggregation: AS69 [30] and chaperones, peptides, and foldamers targeting this region [31–33] inhibit α-syn aggregation; a mutant lacking from residues 36–42 (called "master manipulator" [34]) and 45–57 was shown not to aggregate under physiological pH [34,35]; the so-called preNAC segment (residues 47–56) [15] is critical for cell toxicity and fibril formation. The great significance of this region is emphasized by the fact that many disease-associated mutations are localized here, for instance E46K, H50Q, G51D, A53E and A53T [10,36-39].

CC48 is an intrinsically disordered protein just like WT α-syn, but in contrast to WT α-syn does not aggregate as long as the disulfide bond is closed [28]. It inhibits elongation of WT α-syn fibrils, which could be analyzed with the framework of enzyme inhibition, with the fibril end acting as the enzyme and α-syn monomers corresponding to the substrate [29]. CC48 acted as a competitive inhibitor. Interestingly, monomeric WT α-syn promoted inhibition presumably by stabilizing the blocked state at the fibril end. In line with this, a fusion construct of WT α-syn and CC48 was shown to drastically enhance the inhibitory effect (Fig. 2A). In order to gain further mechanistic insight into α-syn fibril elongation and its inhibition, we here tested which regions of WT-CC48 are responsible for the strong inhibitory effect. For this purpose, we exploited the dimeric nature of the WT-CC48 fusion to generate fusion constructs with deletions of specific regions (Fig. 1) either in the WT or the CC48 part. For this set of truncated versions of WT-CC48 we compared their potential to inhibit fibril elongation. The data demonstrates that the central regions of α-syn, which constitute the fibril core, are also most critical for inhibition of fibril elongation.

Results

Fusion of α-syn WT and the disulfide mutant CC48 inhibits fibril elongation by blocking fibril ends

To test the effect of inhibitors on fibril elongation, we applied a well-established assay in which 2.5 μM pre-formed fibrils (concentration in monomer units) are added to 25 μM α-syn monomers at neutral pH, followed by monitoring of fibril growth under quiescent conditions to suppress nucleation of new fibrils [29,40]. The amount of amyloid is detected using the amyloid specific fluorescent dye, Thioflavin T (ThT), which changes intensity dramatically upon binding to amyloids (Fig. 2B). Inhibition of fibril elongation can be displayed by calculating the ratio of the initial rates of increase in ThT fluorescence with inhibitor (R) vs. without inhibitor (R_0) (Fig. 2C). The dependence of R/R_0 on inhibitor concentration can be explained by a competition of inhibitor and WT substrate for the binding sites at the fibril ends (competitive inhibition model, more specifically the FI model, devised in ref. [29]). In presence of WT-CC48, a complete inhibition of fibril elongation could be detected at nanomolar concentrations (Fig. 2B and C). At the end of the kinetic assay, elongation of the pre-formed fibril seeds was confirmed by atomic force microscopy (AFM), with higher fibril length in the absence of inhibitor (Fig. 2D and E).

In our previous study, we hypothesized that binding of CC48-based inhibitors to the fibril end would lead to a templating-incompetent, i.e., blocked, state [29]. To obtain further evidence for this mechanism, we tested if fibrils lose the ability to elongate upon pre-incubation with WT-CC48 followed by fibril isolation. The pre-formed fibrils were incubated with 25 μM WT-CC48 and as a control with α-syn WT monomers overnight at 37 °C under quiescent conditions. Subsequently, the fibrils were separated by centrifugation and used as pre-formed fibrils in the ThT assay. The sample containing pre-formed fibrils pre-incubated with WT-CC48 did not show any increase in ThT signal, in contrast to the control sample (Fig. 2F). Two conclusions can be drawn from this experiment: *I*) WT-CC48 binds α-syn fibrils with high kinetic stability of the bound state, *II*) WT-CC48 inhibits fibril elongation. This is in line with WT-CC48 inhibiting fibril elongation by capping of fibril ends.

The WT part of WT-CC48 promotes inhibition of fibril elongation due to its HP and NAC regions

To identify the regions of the WT part of WT-CC48 that interact with the fibril end, different truncations of the WT part were generated. Structurally, α-syn is commonly divided into three distinct regions: the amphipathic N-terminus (amino acids 1–60), the central hydrophobic region termed NAC (amino acid 61–95), and the acidic C-terminus (amino acids 96–140) (Fig. 1). In this study, we further subdivided the N-terminus into two parts: The very N-terminus (amino acids 1–31) and the HP region (amino acids 32–60). Our experimental goal was to investigate the relevance of these regions in the inhibitory mechanism of WT-CC48 on fibril elongation. To this purpose, eight fusion constructs were designed in which the N, HP, NAC or C region, or combinations

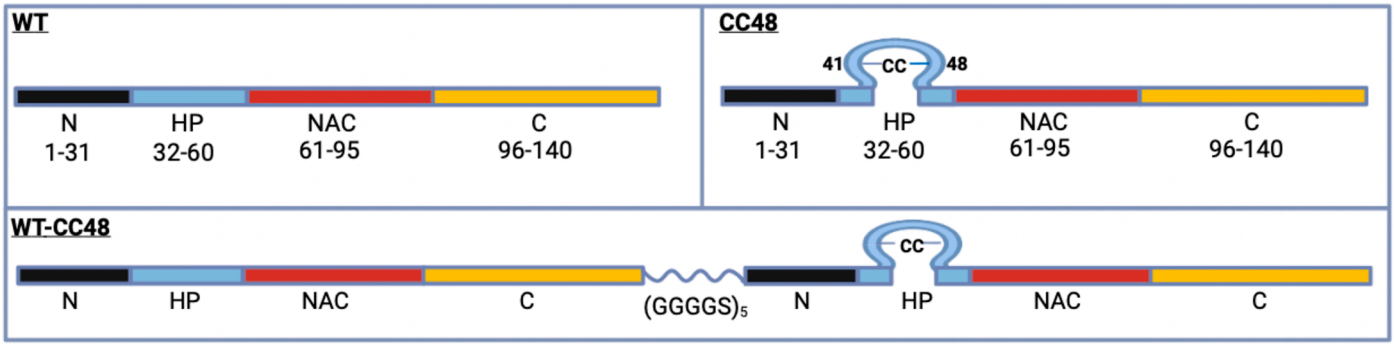

Fig. 1. Wildtype α-synuclein (WT) illustrated by its characteristic regions: N-terminus (N) from residue 1–31 (black), hairpin (HP) from residue 32–60 (blue), non-amyloid-β component (NAC) from residue 61–95 (pink) and C-terminus (C) from residue 96–140 (yellow). The double cysteine mutant CC48 (G41C, V48C) only differs in the HP region (32–60). The WT-CC48-construct is composed of the wildtype sequence linked via a $(G_4S)_5$ linker to CC48. A linker length of 25 amino acids was chosen to ensure sufficient conformational flexibility and length to bridge binding sites at the fibril end.

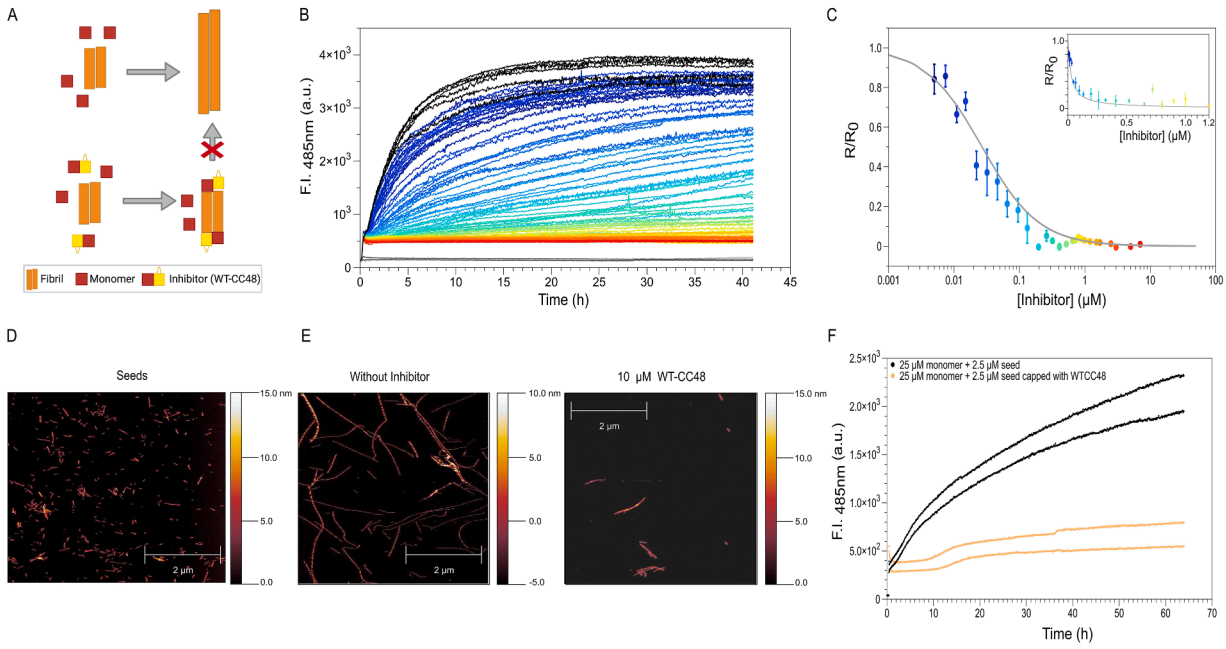

Fig. 2. WT-CC48 inhibits fibril elongation at low substoichiometric ratios. (A) Schematic overview of the suggested mode of action of WT-CC48 [29]. Monomeric α-syn WT is shown as a red square, while the CC48 part is shown as a yellow square with a disulfide-bound. In the presence of pre-formed fibrils monomeric WT can bind to the fibril end and the fibril grows in length. However, in the presence of WT-CC48, WT-CC48 can get incorporated in the fibril structure and stops fibril growth. (B) ThT assay performed at pH 7.4 with 25 μM α-syn WT monomers, 2.5 μM seeds and different inhibitor concentrations between 5 nM and 10 μM, shown in a color gradient from blue to red, under quiescent conditions. The measurement was performed in triplicates. Negative controls are shown in gray shades and positive control (NoWT-CC48) in black. (C) Relative rates of fibril elongation were plotted against the inhibitor concentration (μM) with logarithmic scale or linear scale (inset). The solid line is a fit to a model of competitive inhibition (FI model). (D,E) AFM of (D) fibril seeds and (E) fibrils generated in the ThT assays of α-syn WT without inhibitor and with 10 μM WT-CC48. (F) ThT assay using seeds that were pre-incubated with a 1to1 ratio of WT-CC48 or α-syn WT. Pre-incubation was done overnight and seeds were isolated by centrifugation at 100.000 xg for 1 h. The measurement was performed in duplicates.

thereof, were removed from the WT part of WT-CC48 (Fig. 3).

Truncation of the N-terminus (WTΔN-CC48) did not change the inhibitory strength compared to the full-length construct (Fig. 3A and SI Fig. 1A). However, further removal of the HP region (WTΔNΔHP-CC48) led to a strong reduction of the capability of the inhibitor (Fig. 3A, SI Figure 1B). Additional reduction of inhibitory strength is caused by the deletion of the NAC region (WTΔNΔHPΔNAC-CC48) (Fig. 3A and SI Fig. 1C). Truncation of the C-terminus only (WTΔC-CC48) showed a moderate decrease in inhibition strength, whereas additional deletion of the NAC region (WTΔNACΔC-CC48) strongly decreased inhibition potency (Fig. 3B and SI Fig. 2). From these results we infer that the removal of the NAC and HP regions lead to strong reductions in inhibition of fibril elongation. However, the removal of the N or C termini has only minor effects, which was confirmed by a fusion construct which lacks both termini (WTΔNΔC-CC48) (Fig. 3C and SI Fig. 3A). This construct shows the same inhibitory efficiency as full-length WT-CC48. Interestingly, removal of either the HP or NAC region reduced the inhibitory effect of the fusion construct dramatically, indicating that both regions are required for potent inhibition (Fig. 3C and SI Fig. 3B and C).

The inhibitory effects observed in the kinetic assay were confirmed by sucrose density gradient centrifugation (DGC) and AFM. Size distribution analysis by DGC showed that α-syn in the absence of inhibitor formed high molecular weight (HMW) assemblies which sedimented in the bottom fractions (Fig. 4A). AFM confirmed that these aggregates were amyloid fibrils (Fig. 4A). 10 μM WTΔC-CC48, with only the C-terminus removed, ensured that α-syn remained predominantly in monomeric form (Fig. 4B). The less effective inhibitor WTΔNΔNACΔC-CC48, which lacks the important NAC region, retained α-syn only partially in monomeric form (Fig. 4C).

The HP and NAC regions of also the CC48 part of WT-CC48 are crucial for strong inhibition of fibril elongation

The inhibitor CC48 differs from WT monomer only by the introduction of two cysteines at position 41 and 48 and retains the intrinsically disordered nature of WT α-syn [28]. The fusion of the inhibitor CC48 and its co-inhibitor, WT, increases the inhibition strength [29]. Assuming that WT promotes inhibition by binding to fibril ends, the question arises whether the binding of the structurally similar CC48 to fibril ends occurs by the same mechanism. We wondered whether removal of the different regions in the CC48 part had the same effect on inhibition as truncation of the corresponding regions in the WT part. In one of the constructs, the C-terminal and N-terminal region of the CC48 part were removed (WT-CC48ΔNΔC). For this construct, the inhibition is in the same nanomolar range as for the full-length construct (Fig. 5 and SI Fig. 4A). In contrast, additional removal of the NAC (WT-CC48ΔNΔNACΔC) region decreased the inhibitory effect (Fig. 5 and SI Fig. 4B). We finally compared the effects of truncations of corresponding regions in the two parts of the fusion construct, WT or CC48. Deletion of N- and C-terminus in either the WT or the CC48 part did not have a clear effect on the inhibitory potential (SI Fig. 5A). However, the NAC region is required in both parts to maintain their high inhibitory potency (SI Fig. 5B). Thus, we suggest that both, the WT part and the CC48 part, require the NAC and HP regions for optimal interaction with the protofilaments' cross-β core interfaces at the fibril end.

As a control experiment, we investigated two concentrations of all constructs on the same microtiter plate using the same seed preparation in a ThT experiment (SI Fig. 6A–E) to ensure that any observed differences in inhibitory activity were not due to or compromised by differences between seed preparations. In addition, the insoluble vs. soluble fractions post aggregation were analyzed by ultracentrifugation followed by SDS-PAGE (SI Fig. 6F–I). The data confirmed the previous

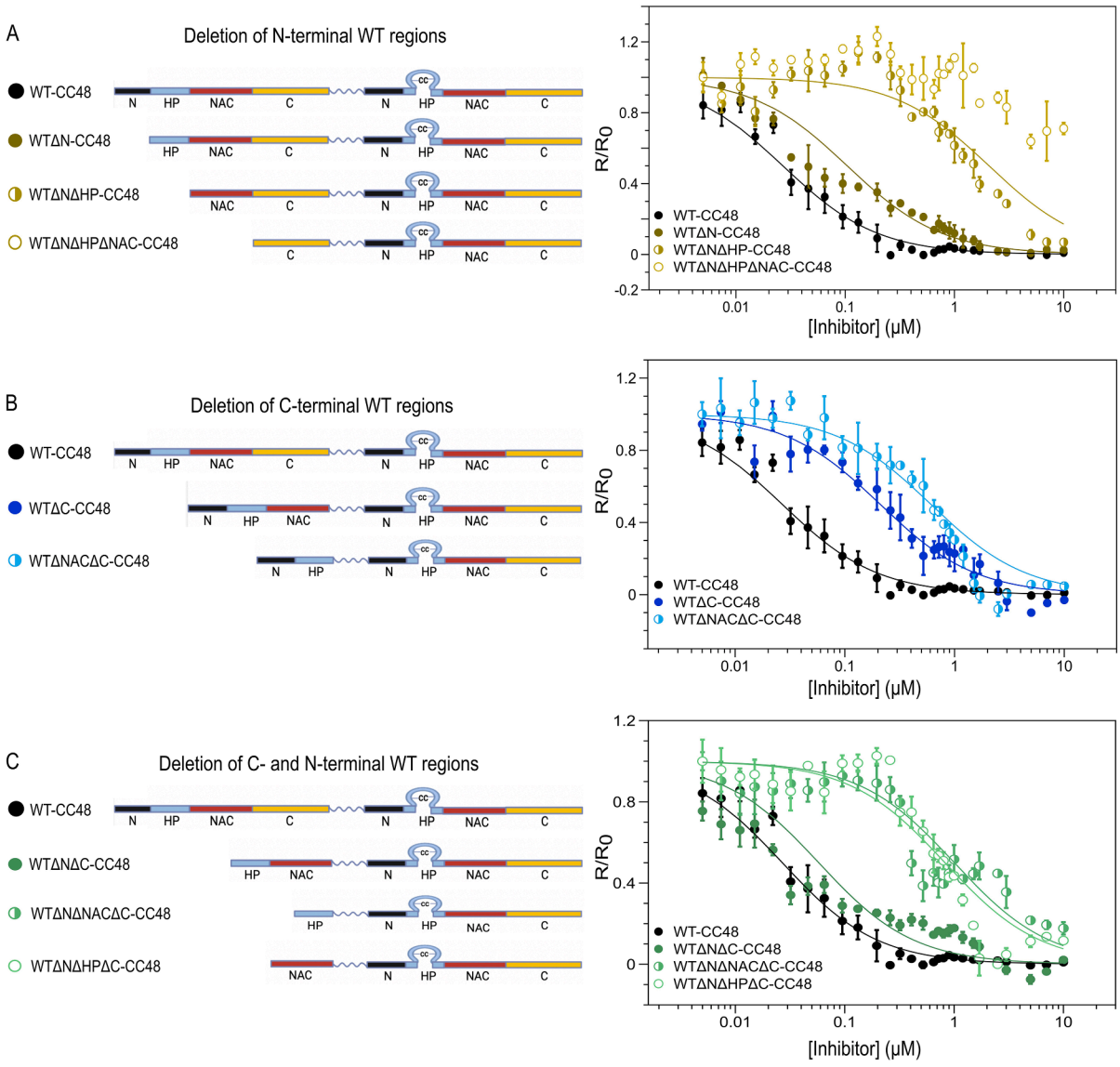

Fig. 3. Truncations of α-syn WT regions in WT-CC48 affect inhibition of fibril elongation. Left, Schematic representation of the constructs visualizes the truncation of the N-terminal WT regions (A), the deletion of the C-terminal WT regions (B) and the deletion of both C- and N-terminal WT regions (C). The individual α-syn regions are displayed in different colors: N-terminus (residues 1–31) in black, hairpin region (residues 32–60) in blue, NAC region (residues 61–95) in pink and the C-terminus (residues 96–140) in yellow. The HP region of the CC48 part is shown as a loop. Right, relative rates of fibril elongation obtained from elongation assays (SI Figures 1–3) were plotted against the inhibitor concentration (μM). For the constructs WTΔNΔHPΔNAC-CC48, WTΔNΔHP-CC48, WTΔNACΔC-CC48, WTΔNΔNACΔC-CC48, and WTΔNΔHPΔC-CC48 the r/r0 values were normalized to 1.0 for the lowest inhibitor concentration, as the R/R_0 values at low inhibitor concentrations were stable at a value above 1.0 for these constructs (see SI Figures 1–3 for the non-normalized data). Solid lines are fits to a model of competitive inhibition (FI model).

observations regarding the relative inhibitory activity of the different fusion constructs.

Discussion

In this study we could confirm that WT-CC48 is a potent inhibitor of fibril elongation of α-syn. Comparing the IC50 values of all investigated constructs, we find that all constructs containing the HP and the NAC region in both WT and CC48 part show strong inhibition similar to that of full-length WT-CC48 (Fig. 6A). This indicates that both, the HP and the NAC region (together residues 32–95), of both, the WT and CC48 part of the fusion construct, are necessary for the nanomolar inhibitory strength. In contrast, the N- and C-termini do not play an important role in CC48-mediatied inhibition of fibril elongation (Fig. 6A). Regardless of the fibril polymorph, the region between residues 32–95 lies in the fibril core [15,41-47]. At the fibril ends, this region exposes the open cross-β structure as an interface for monomer attachment and as a template for their conversion into the fibril conformation. Since almost all α-syn fibril polymorphs reported to date consist of two protofilaments, this open cross-β structure interface extends over two HP and NAC regions (Fig. 6B). The observation that two HP and two NAC regions are required to maximize inhibition suggests that the full cross-β interface can be recruited for interaction with the inhibitor WT-CC48.

The data obtained here for the WT-CC48 fusion constructs allows to refine a model describing how CC48 achieves inhibition of fibril elongation, and how WT molecules support this activity. The model is illustrated in Fig. 7, in which CC48 corresponds to the inhibitor (yellow), whereas the supportive WT molecules are displayed in red. Note that the WT-CC48 fusion would in this scheme correspond to the linkage of the yellow CC48 inhibitor with a red WT molecule. The fact that the same

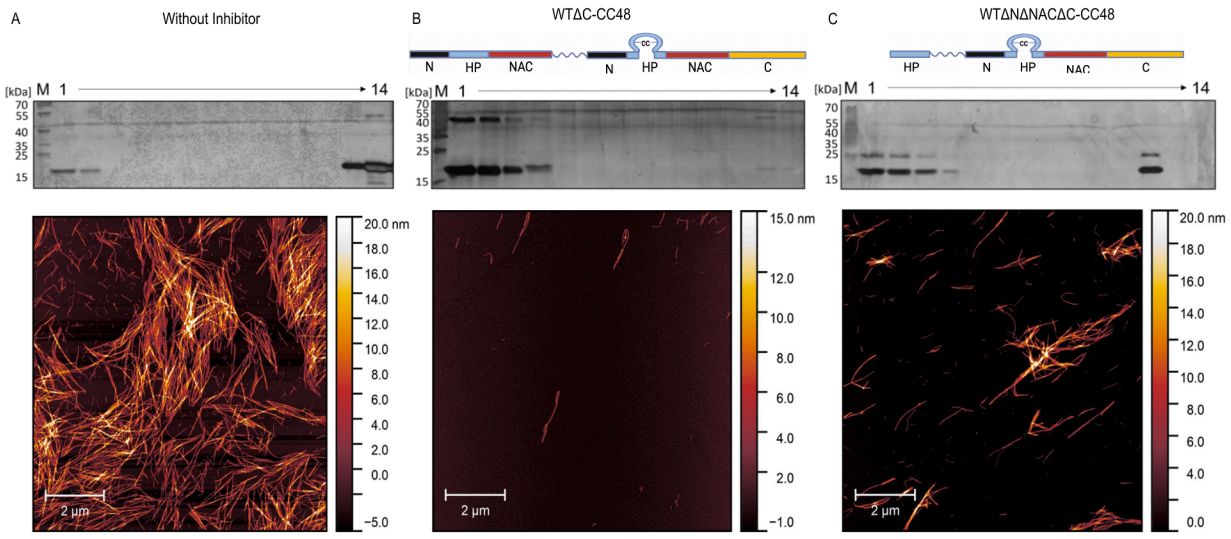

Fig. 4. Different efficiency of inhibition of fibril elongation of truncated WT-CC48 constructs. Sucrose DGC and AFM imaging of samples at the end of the kinetic aggregation for α-syn WT without inhibitor (A), with 10 μM WTΔC-CC48 (B), or with 10 μM WTΔNΔNACΔC-CC48 (C). DGC fractions, analysed by SDS-PAGE (15% tris-glycine gel), are numbered from 1 to 14, with low-density fractions given lower numbers and higher density fractions higher numbers. M, marker. α-syn monomers are obtained in low-density fractions 1–4, whereas α-syn aggregates are found in high-density fractions 12–14 [50]. In SDS-PAGE, α-syn runs at an apparent MW of ~17 kDa. WTΔC-CC48 and WTΔNΔNACΔC-CC48 co-migrate with α-syn in DGC and run in SDS-PAGE at apparent MWs of ~45 and 25 kDa, respectively.

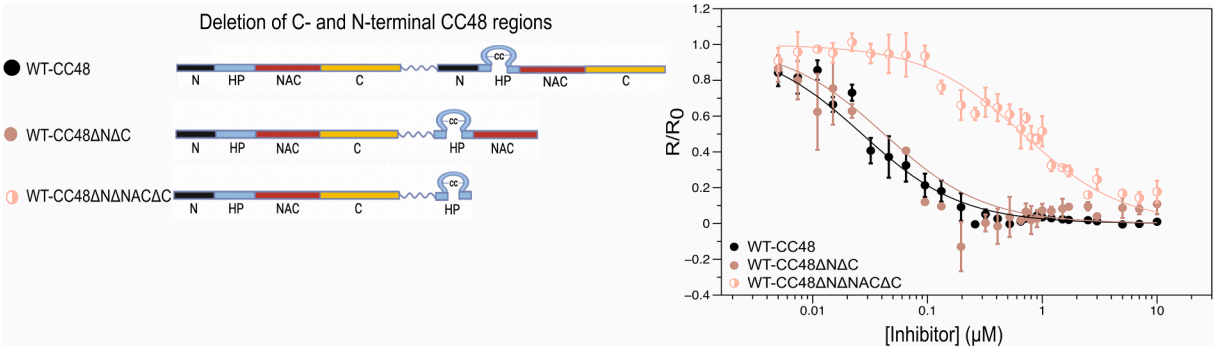

Fig. 5. Truncations of CC48 regions of WT-CC48 affect inhibition of fibril elongation. Left, schematic representation of the constructs visualizes the deletion of C- and N-terminal regions. The different regions of α-syn are displayed in different colors: N-terminus (residues 1–31) in black, hairpin region (residues 32–60) in blue, NAC region (residues 61–95) in pink and the C-terminus (residues 96–140) in yellow. The HP region of the CC48 part is shown as a loop. Right, relative rates of fibril elongation obtained from elongation assays (SI Fig. 4) were plotted against the inhibitor concentration (μM). Solid lines are fits to a model of competitive inhibition (FI model).

regions are required for fibril inhibition as for fibril elongation supports a model in which CC48 establishes similar interactions with the fibril end as WT monomers but prohibits conformational conversion into the templating-competent structure of the seed fibril (Fig. 7). CC48 may bind to one protofilament, engaging in largely the same interactions as a WT monomer would (Fig. 7, point 2). A WT monomer can bind to the second protofilament and stabilize the CC48-bound state. However, due to the presence of CC48, it does not adopt precisely the same conformation as the other WT units in the seed fibrils, resulting in a fibril end that is not anymore templating-competent (Fig. 7, point 3). Kinetic analysis previously suggested that even more than one WT unit supports fibril end blocking [29]. This can be explained by formation of an oligomer-like cap, consisting of a few α-syn molecules, on the fibril end (Fig. 7, point 4). By the direct linkage of CC48 with WT within the fusion constructs, their cooperative action is exploited to achieve blocking of fibril ends at two orders of magnitude lower inhibitor concentration than for CC48 alone [29].

The strategy applied here to interfere with fibril formation is based on recruitment of self-interactions between an amyloidogenic protein and an inhibitor that is a modified version thereof. The results indicate that for this type of inhibitor rather large protein segments are required to achieve sufficient inhibition activity. In the case of α-syn, we find that the HP and NAC regions are important to maximize the inhibitory efficiency. The particular need for HP and NAC once again highlights the role of self-interactions in amyloid assembly and inhibition. Fusion of the HP and NAC regions of WT α-syn might be a useful strategy to improve the activity of fibril elongation inhibitors.

Materials and methods

Transformation, expression and purification of α-syn and WT-CC48 variants

α-syn was encoded in the expression vector pT7–7 and expressed in *Escherichia coli* (*E. coli*) strain BL21(DE3). The WT-CC48 variants were encoded in the expression vector pET11-a purchased from GenScript Biotech and expressed in *E. coli* BL21(DE3). For transformation, the cells were thawed on ice for 10 min. Then, 10 ng of the plasmid was added to

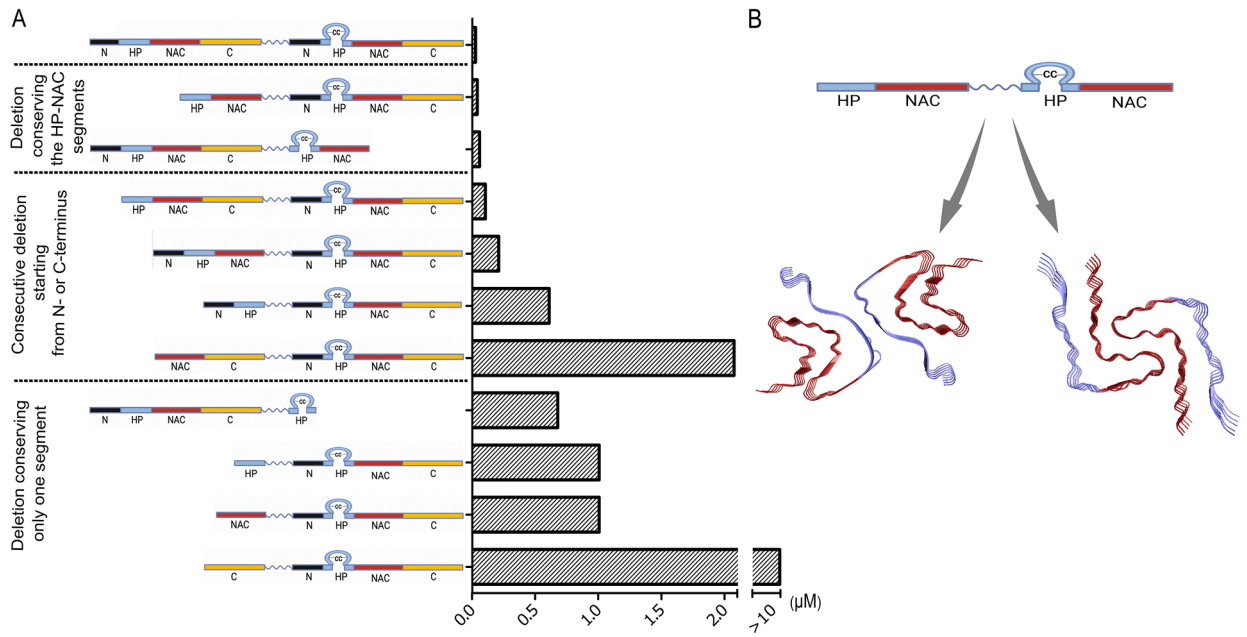

Fig. 6. Overview of important regions in WT-CC48 for inhibition of fibril elongation. (A) IC50 values of the investigated constructs derived from the fits to the competitive inhibition model. (B) From the data, it can be concluded that in both parts of the constructs, WT and CC48, the HP and the NAC region are of great importance for the inhibition of the α-syn fibril elongation. Both parts, HP and NAC region, build the fibrillar core of α-syn fibrils, suggesting that elongation is driven by self-interactions between HP and NAC regions at the fibril end and in the inhibitor. The polymorphs shown here are taken from [15], PDB codes 6CU7 (rod polymorph) and 6CU8 (twister polymorph).

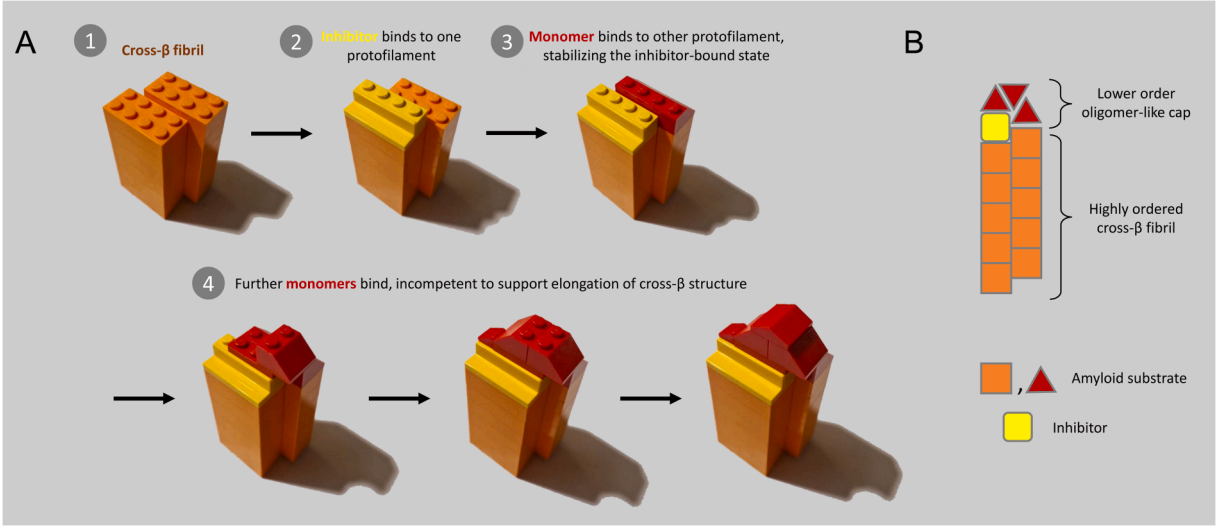

Fig. 7. Model of CC48-mediated inhibition of fibril elongation. In this scheme, CC48 corresponds to the inhibitor (yellow), whereas the supportive WT molecules are displayed in red. Note that the WT-CC48 fusion would in this scheme correspond to the linkage of the yellow CC48 inhibitor with a red WT molecule. 1) α-syn fibril polymorphs typically consist of two protofilaments, each exposing at the fibril end an open cross-β interface (pins on the click brick) consisting of HP and NAC region. 2) CC48 (yellow) may bind to one protofilament, engaging in largely the same interactions as a WT monomer (orange) would. 3) WT monomer (red) can bind to the second protofilament, stabilizing the CC48-bound state that is incompetent to template further elongation of the ordered fibril structure. 4) Further WT monomers can add to the fibril end, creating an oligomer-like cap.

the cells and incubated on ice for another 10 min. After that, heat shock was performed by heating the cells to 42 °C for 60 s. The cells were immediately placed on ice again for 2 min. Preheated (37 °C) LB medium was added to the cells, and they were incubated at 37 °C 800 rpm for 1 h. The cells were plated on LB-agar plates supplemented with 100 μg/ml ampicillin and incubated at 37 °C overnight. The next day, a preculture of 50 ml 2YT supplemented with 100 μg/ml ampicillin was prepared and incubated at 37 °C and 160 rpm overnight. The next day, the main culture (500 ml in a 2 l Erlenmeyer flask) was inoculated with 5 ml of the preculture. It was incubated at 37 °C and 110 rpm until an OD_{600} of 0.6 was reached and induced with a final concentration of 1 mM IPTG. The culture was incubated for growth for 4 h at 37 °C and 110 rpm. The cells were harvested at 5000 x g, 4 °C for 20 min. The supernatant was discarded. The pellet was resuspended in 10 ml distilled water. Protease inhibitor was added. The cells were frozen at −20 °C. α-syn and fusion constructs were purified as described previously [29,40,48].

Elongation assay

For seed preparation 25 μM of α-syn, 20 μM ThT, 0.04% NaN_3 and 20 mM MOPS pH 7.4, 50 mM NaCl were incubated in a volume of 1 ml with an added glass bead at 37 °C at 800 rpm for 72 h. Before addition to the 96-well plate, the seeds were pipetted to a 2 ml Eppendorf tube and sonicated at 70% for 30 s twice using UP200St Ultrasonic Processor from Hielscher.

In the elongation assay 25 μM α-syn monomers supplemented with 20 μM ThT, 0.04% NaN_3 in 20 mM MOPS pH 7.4, 50 mM NaCl were incubated with different concentration of the WT-CC48 constructs. Seeds were added to a final concentration of 2.5 μM. As controls, the seeded monomer without any WT-CC48 construct, the unseeded monomer without any WT-CC48 construct, the WT-CC48 constructs only, and the seeds only were used. All components except for the seeds were added to a 96-well half-area, non-binding surface, black with clear bottom, polystyrene plate (3881, Corning) and incubated at 37 °C for 10 min. Then, the sonicated seeds were added to start the elongation kinetics. The ThT fluorescence was observed over 40 h. The ThT signal was measured at 482 nm after excitation at 448 nm in a BMG FLUOstar Omega platereader. Measurements were done every 100 s in cycle 1 to 110 and every 300 s in the following cycles. The fluorescence measurement was set in a ring with 12 points with a diameter of 3 mm.

For evaluation of elongation kinetics, the slope in the initial stages of the experiment (i.e., in the time window between 1 and 3 h after addition of seeds to monomers) was calculated, yielding the rate R. For comparing inhibitory activity between fibril elongation samples containing different seed preparation, we found it imperative to normalize the elongation rate to that of an uninhibited control (R_0), yielding R/R_0 [29]. Some of the constructs exhibited R/R_0 values consistently above 1.0 at low inhibitor concentrations. We normalized these R/R_0 data sets to a value of 1.0 for the lowest inhibitor concentration investigated. The non-normalized R/R_0 data is shown in the SI.

The R/R_0 data was fitted to a model of competitive inhibition (FI model), assuming that the inhibitor competes with WT molecules for the fibril end [29]:

$$\frac{R}{R_0} = \frac{K_m + [M]}{[M] + K_m\left(1 + \frac{[I]}{K_i}\right)}$$

K_m and K_i are the dissociation constants of WT monomer or inhibitior, respectively, binding to the fibril end, and [M] and [I] are the concentrations of WT monomer and inhibitor, respectively. IC50 values were obtained from the fits to the FI model.

In the elongation assay with WT-CC48 with capped seeds, 25 μM WT-CC48 were incubated with 25 μM (monomer concentration) pre-formed fibrils overnight at 37 °C, 800 rpm. The seeds were spun down for 1 h at 100,000 x g. The supernatant was discarded, and the pellet resuspended in 20 mM MOPS pH 7.4, 50 mM NaCl supplemented with 20 μM ThT and 0.04% NaN_3. The elongation assay was prepared as described above.

Preparation and SDS-PAGE of soluble and insoluble fractions after elongation assay

After the elongation assay serving as a further control (inhibitor concentrations: 0.5 μM and 5 μM), the soluble and the insoluble fractions were separated by ultracentrifugation at 100,000 x g for 1 h. The supernatant was transferred to a new reaction tube and the pellet resolved in 20 mM MOPS pH 7.4, 50 mM NaCl in a volume equivalent to the volume of the supernatant. The samples were diluted 1:4 with SDS-loading buffer (200 mM Tris–HCl pH 6.8, 400 mM DTT, 8% SDS, 0.4% bromophenol blue, 40% glycerol) followed by 15% Tris-Glycine-SDS-PAGE. PageRuler Protein Ladder was used. Gel electrophoresis was performed at 120 V.

Density gradient centrifugation (DGC) and SDS-PAGE

The samples from the 96-well plates after ThT measurements were taken and loaded on a discontinuous sucrose gradient and centrifuged for 3 h at 259,000 x g at 4 °C in a TLS-55 rotor (Beckmann). The sucrose gradient (as described in [49]) contained the following volumes and concentrations (w/w, from bottom to top): 300 μl of 60%, 200 μl of 50%, 200 μl of 25%, 400 μl of 20%, 400 μl of 15%, 150 μl of 10% and 400 μl of 5%. The gradient was layered stepwise in a 11 × 34 mm polyallomer centrifuge tube (Beckmann). After fractionating the gradient, each fraction was diluted 1:6 with SDS-loading buffer (50 mM Tris–HCl pH 7.4, 12% glycerol, 4% SDS, 2% β-mercaptoethanol) and analysed by 15% Tris-Glycine-SDS-PAGE. PageRuler Protein Ladder was used. Gel electrophoresis was performed at 120 V.

Atomic force microscopy (AFM)

AFM images were taken with a Bruker Multimode 8 microscope with ScanAsyst-Air cantilevers using the ScanAsyst PeakForce Tapping Mode in air. 10 μl of the protein solution was applied to a freshly cleaved mica and incubated for 10 min at RT under humified conditions. The sample was washed with 100 μl distilled water five times. Then, the sample was dried using gaseous N_2. The software Gwyddion was used for processing the AFM images.

CRediT authorship contribution statement

Celina M. Schulz: Conceptualization, Data curation, Investigation, Visualization, Writing – original draft, Writing – review & editing. **Anne Pfitzer:** Conceptualization, Data curation, Investigation, Visualization, Writing – original draft, Writing – review & editing. **Wolfgang Hoyer:** Conceptualization, Data curation, Supervision, Visualization, Writing – review & editing.

Declaration of Competing Interest

The authors declare the following financial interests/personal relationships which may be considered as potential competing interests:

Wolfgang Hoyer reports financial support was provided by European Research Council. Anne Pfitzer reports financial support was provided by Jürgen Manchot Foundation.

Data availability

Data will be made available on request.

Acknowledgments

This project has received funding from the European Research Council under the European Union's Horizon 2020 research and innovation program, grant agreement no. 726368. AP thanks the Jürgen Manchot Foundation for funding. Figures were partially created with BioRender.com.

Supplementary materials

Supplementary material associated with this article can be found, in the online version, at doi:10.1016/j.bbadva.2023.100110.

References

[1] F. Chiti, C.M. Dobson, Protein misfolding, amyloid formation, and human disease: a summary of progress over the last decade, Annu. Rev. Biochem. 86 (2017) 27–68.
[2] H. Olzscha, et al., Amyloid-like aggregates sequester numerous metastable proteins with essential cellular functions, Cell 144 (1) (2011) 67–78.

[3] R.M. Vabulas, F.U. Hartl, Aberrant protein interactions in amyloid disease, Cell Cycle 10 (10) (2011) 1512–1513.
[4] C.M. Dobson, Protein misfolding, evolution and disease, Trend. Biochem. Sci. 24 (9) (1999) 329–332.
[5] E. Chuang, et al., Amyloid assembly and disassembly, J. Cell Sci. (8) (2018) 131.
[6] F. Chiti, C.M. Dobson, Protein misfolding, functional amyloid, and human disease, Annu. Rev. Biochem. 75 (2006) 333–366.
[7] P. Westermark, et al., Amyloid: toward terminology clarification Report from the Nomenclature Committee of the International Society of Amyloidosis, Amyloid 12 (1) (2005) 1–4.
[8] A.B. Reiss, et al., Amyloid toxicity in Alzheimer's disease, Rev. Neurosci. 29 (6) (2018) 613–627.
[9] D. Aarsland, et al., Cognitive decline in Parkinson disease, Nat. Rev. Neurol. 13 (4) (2017) 217–231.
[10] M.H. Polymeropoulos, et al., Mutation in the α-synuclein gene identified in families with Parkinson's disease, Science 276 (5321) (1997) 2045–2047.
[11] M.G. Spillantini, et al., α-Synuclein in filamentous inclusions of Lewy bodies from Parkinson's disease and dementia with Lewy bodies, Proc. Natl Acad. Sci. 95 (11) (1998) 6469–6473.
[12] L. Bousset, et al., Structural and functional characterization of two alpha-synuclein strains, Nat. Commun. 4 (1) (2013) 2575.
[13] J. Verasdonck, et al., Further exploration of the conformational space of α-synuclein fibrils: solid-state NMR assignment of a high-pH polymorph, Biomol. NMR Assign. 10 (1) (2016) 5–12.
[14] A. Makky, et al., Nanomechanical properties of distinct fibrillar polymorphs of the protein α-synuclein, Sci. Rep. 6 (1) (2016) 1–10.
[15] B. Li, et al., Cryo-EM of full-length α-synuclein reveals fibril polymorphs with a common structural kernel, Nat. Commun. 9 (1) (2018) 3609.
[16] M.G. Iadanza, et al., A new era for understanding amyloid structures and disease, Nat. Rev. Mol. Cell Biol. 19 (12) (2018) 755–773.
[17] T.P.J. Knowles, M. Vendruscolo, C.M. Dobson, The amyloid state and its association with protein misfolding diseases, Nat. Rev. Mol. Cell Biol. 15 (6) (2014) 384–396.
[18] M. Törnquist, et al., Secondary nucleation in amyloid formation, Chem. Commun. 54 (63) (2018) 8667–8684.
[19] J.D. Camino, P. Gracia, N. Cremades, The role of water in the primary nucleation of protein amyloid aggregation, Biophys. Chem. 269 (2021), 106520.
[20] S. Linse, Mechanism of amyloid protein aggregation and the role of inhibitors, Pure Appl. Chem. 91 (2) (2019) 211–229.
[21] A.K. Buell, The growth of amyloid fibrils: rates and mechanisms, Biochem. J. 476 (19) (2019) 2677–2703.
[22] P. Arosio, et al., Chemical kinetics for drug discovery to combat protein aggregation diseases, Trend. Pharmacol. Sci. 35 (3) (2014) 127–135.
[23] P. Sormanni, F.A. Aprile, M. Vendruscolo, Rational design of antibodies targeting specific epitopes within intrinsically disordered proteins, Proc. Natl. Acad. Sci. U.S. A. 112 (32) (2015) 9902–9907.
[24] S. Sangwan, et al., Inhibition of synucleinopathic seeding by rationally designed inhibitors, eLife 9 (2020).
[25] Y.A. Kyriukha, et al., α-synuclein dimers as potent inhibitors of fibrillization, J. Med. Chem. 62 (22) (2019) 10342–10351.
[26] K. Afitska, et al., Structural optimization of inhibitors of α-synuclein fibril growth: affinity to the fibril end as a crucial factor, J. Mol. Biol. 432 (4) (2020) 967–977.
[27] K.A. Murray, et al., De novo designed protein inhibitors of amyloid aggregation and seeding, Proc. Natl. Acad. Sci. USA. 119 (34) (2022), e2206240119.
[28] H. Shaykhalishahi, et al., Contact between the β1 and β2 segments of α-synuclein that inhibits amyloid formation, Angew. Chem. Int. Ed. 54 (30) (2015) 8837–8840.
[29] E.D. Agerschou, et al., Inhibitor and substrate cooperate to inhibit amyloid fibril elongation of α-synuclein, Chem. Sci. 11 (41) (2020) 11331–11337.
[30] E.A. Mirecka, et al., Sequestration of a β-hairpin for control of α-synuclein aggregation, Angew. Chem. Int. Ed Engl. 53 (16) (2014) 4227–4230.
[31] Z. Liang, et al., A SUMO1-derived peptide targeting SUMO-interacting motif inhibits α-synuclein aggregation, Cell Chem Biol 28 (2) (2021) 180–190, e6.
[32] J. Ahmed, et al., Foldamers reveal and validate therapeutic targets associated with toxic α-synuclein self-assembly, Nat. Commun. 13 (1) (2022) 2273.
[33] B.M. Burmann, et al., Regulation of α-synuclein by chaperones in mammalian cells, Nature 577 (7788) (2020) 127–132.
[34] C.P.A. Doherty, et al., A short motif in the N-terminal region of α-synuclein is critical for both aggregation and function, Nat. Struct. Mol. Biol. 27 (3) (2020) 249–259.
[35] S. Lesage, et al., G51D α-synuclein mutation causes a novel Parkinsonian–pyramidal syndrome, Ann. Neurol. 73 (4) (2013) 459–471.
[36] J.J. Zarranz, et al., The new mutation, E46K, of α-synuclein causes parkinson and Lewy body dementia, Ann. Neurol. 55 (2) (2004) 164–173.
[37] S. Appel-Cresswell, et al., Alpha-synuclein p.H50Q, a novel pathogenic mutation for Parkinson's disease, Mov. Disord. 28 (6) (2013) 811–813.
[38] P. Pasanen, et al., A novel α-synuclein mutation A53E associated with atypical multiple system atrophy and Parkinson's disease-type pathology, Neurobiol. Aging 35 (9) (2014) 2180.e1–2180.e5.
[39] M.G. Spillantini, et al., α-Synuclein in Lewy bodies, Nature 388 (6645) (1997) 839–840.
[40] A.K. Buell, et al., Solution conditions determine the relative importance of nucleation and growth processes in α-synuclein aggregation, Proc. Natl. Acad. Sci. U.S.A. 111 (21) (2014) 7671–7676.
[41] M. Schweighauser, et al., Structures of α-synuclein filaments from multiple system atrophy, Nature 585 (7825) (2020) 464–469.
[42] Y. Li, et al., Amyloid fibril structure of α-synuclein determined by cryo-electron microscopy, Cell Res. 28 (9) (2018) 897–903.
[43] R. Guerrero-Ferreira, et al., Two new polymorphic structures of human full-length alpha-synuclein fibrils solved by cryo-electron microscopy, eLife 8 (2019) e48907.
[44] Y. Sun, et al., Cryo-EM structure of full-length α-synuclein amyloid fibril with Parkinson's disease familial A53T mutation, Cell Res. 30 (4) (2020) 360–362.
[45] K. Zhao, et al., Parkinson's disease associated mutation E46K of α-synuclein triggers the formation of a distinct fibril structure, Nat. Commun. 11 (1) (2020) 2643.
[46] D.R. Boyer, et al., The α-synuclein hereditary mutation E46K unlocks a more stable, pathogenic fibril structure, Proc. Natl Acad. Sci. 117 (7) (2020) 3592–3602.
[47] K. Zhao, et al., Parkinson's disease-related phosphorylation at Tyr39 rearranges α-synuclein amyloid fibril structure revealed by cryo-EM, Proc. Natl Acad. Sci. 117 (33) (2020) 20305–20315.
[48] W. Hoyer, et al., Dependence of α-synuclein aggregate morphology on solution conditions, J. Mol. Biol. 322 (2) (2002) 383–393.
[49] N.S. Rösener, et al., A D-enantiomeric peptide interferes with heteroassociation of amyloid-β oligomers and prion protein, J. Biol. Chem. 293 (41) (2018) 15748–15764.
[50] N.S. Rösener, et al., Clustering of human prion protein and α-synuclein oligomers requires the prion protein N-terminus, Commun. Biol. 3 (1) (2020) 365.